Materials Research Bulletin 83 (2016) 623–631

Contents lists available at ScienceDirect

Materials Research Bulletin

journal homepage: www.elsevier.com/locate/matresbu

A comparative study of direct versus post-synthesis alumination of mesoporous FSM-16 silica

M. Zimowska[a], A. Michalik-Zym[a], J. Kryściak-Czerwenka[a], R. Dula[a], R.P. Socha[a], K. Pamin[a], M. Bazarnik[b], K. Bahranowski[c], Z. Olejniczak[d], L. Lityńska-Dobrzyńska[e], E.M. Serwicka[a,*]

[a] Jerzy Haber Institute of Catalysis and Surface Chemistry, Polish Academy of Sciences, ul. Niezapominajek 8, 30-239 Krakow, Poland
[b] Cracow University of Technology, Faculty of Civil Engineering, ul. Warszawska 24, 31-155 Krakow, Poland
[c] Faculty of Geology, Geophysics and Environmental Protection, AGH-University of Science and Technology, al. Mickiewicza 30, 30-059 Krakow, Poland
[d] Institute of Nuclear Physics, Polish Academy of Sciences, ul. Radzikowskiego 152, 31-342 Krakow, Poland
[e] Institute of Metallurgy and Material Chemistry, Polish Academy of Sciences, ul. Reymonta 9, 30-059 Krakow, Poland

ARTICLE INFO

Article history:
Received 21 April 2016
Received in revised form 24 June 2016
Accepted 13 July 2016
Available online 15 July 2016

Keywords:
FSM-16
Mesoporous silica
Alumination
Al distribution
Acidity

ABSTRACT

Al-FSM-16 mesoporous silicas were synthesized either by direct method, from Al-kanemite (Al-FSM-16/D), or by post-synthesis impregnation of purely siliceous FSM-16 with $Al(NO_3)_3$ (Al-FSM-16/P) and characterized with XRD, XRF, SEM, TEM, nitrogen sorption isotherms, ^{27}Al and ^{29}Si MAS NMR, FTIR, XPS, NH_3-TPD, FTIR of pyridine adsorption and catalytic decomposition of ethanol. Only substitutional Al sites exist in Al-FSM-16/D, while in Al-FSM-16/P some Al remains in extra-lattice positions. Upon transformation of Al-FSM-16/D into hydrogen form a certain amount of extra-framework Al is formed. Direct alumination introduces a higher degree of structural disorder. In Al-FSM-16/D, Al is preferentially accumulated at inner pore walls, while in Al-FSM-16/P external surface is Al-rich. Post-synthesis alumination is more efficient in introducing acid sites into FSM-16. The generated acidity is of Brønsted and Lewis nature, the latter being stronger than the former.

1. Introduction

Ordered mesoporous silicas represent an important class of porous structures with well defined pores of controlled dimensions, shape and connectivity. The materials find many applications, particularly in the field of catalysis, separation processes, and host-guest chemistry. Alumination of the mesoporous silicas is one of the most popular method of their modification. Isomorphous substitution of Al for Si aims at development of cation exchange/acid properties, and extends further potential of these materials as hosts, adsorbents or catalysts. Formation of Al-containing ordered mesoporous silica frameworks had already been described in the 1992 reports on the syntheses of MCM-41 [1], and the material referred to later as FSM-16 [2]. FSM-16 silicas, derived from kanemite, a layered sodium silicate of the formula $NaHSi_2O_5 \times 3 H_2O$, are structurally analogous to the extensively studied MCM-41 materials, as they are highly ordered mesoporous solids with a hexagonal array of uniform channels, high specific surface area and pore volume [3].

Insertion of aluminum into mesoporous silicas is usually carried out by one of the two well established synthesis routes: direct method, consisting in addition of Al source to the synthesis gel, or post-synthesis treatment, in which Al source is incorporated into purely siliceous mesoporous framework by such means as grafting or impregnation. The literature on MCM-41 alumination by either of the procedures is plentiful [1,2,4–32], and includes many studies comparing the effects of direct versus post-synthesis alumination [20–32]. It has been shown that the method of Al insertion determines the material structure, stability, Al distribution, acidity and catalytic properties.

In contrast to copious findings related to MCM-41 aluminosilicates, the reports investigating the effect of alumination on FSM-16 structure and properties are much fewer [2,33–39]. It should be noted, that despite close structural similarities between MCM-41 and FSM-16, the materials are formed via essentially different mechanisms [40–42]. The cooperative self-assembly of surfactant and a dissolved silica source, operating during the synthesis of MCM-41, leads to a direct build up of the hexagonal mesophase

* Corresponding author.
E-mail address: ncserwic@cyf-kr.edu.pl (E.M. Serwicka).

http://dx.doi.org/10.1016/j.materresbull.2016.07.016
0025-5408/

without formation of any transient ordered silicate-surfactant phases. In contrast, transformation of kanemite, exchanged with surfactant cations, to FSM-16, involves ordering of fragmented anionic silicate sheets into an intermediate layered silica-surfactant mesophase, followed by subsequent evolution of the actual hexagonal structure. Comparative studies of purely siliceous forms of MCM-41 and FSM-16 revealed that some properties of these structurally related materials show considerable differences. Thus, it has been observed that FSM-16 solids have higher thermal and hydrothermal stability than MCM-41 ones [43,44], the effect attributed to a higher degree of condensation within the pore walls of the former. Also, comparison of photocatalytic activity of FSM-16 and MCM-41 in several organic transformations demonstrated superiority of the kanemite-derived mesoporous silica catalyst [45].

In view of the above, and considering the uniqueness of the self assembly process leading to the FSM-16 structure, we decided to investigate in more detail the process of Al insertion into the structure of FSM-16, focusing on the role of the employed alumination route and the effect it has on the structure, texture, Al localization and evolution of the acid function of the resulting solids.

2. Experimental

2.1. Materials

Kanemite was synthesized from water glass (Aldrich, reagent grade, molecular formula $Na_2Si_3O_7$), following the procedure optimized in our laboratory [46,47]. Briefly, the Na/Si ratio was adjusted to 1 by addition of appropriate amount of 2 M NaOH solution. The liquid was dried in air at 100 °C for 24 h and the remaining solid calcined at 700 °C for 1 h, ground, and stirred in water for 10 min, to yield kanemite. The FSM −16 solids were obtained according to the method originally proposed by Inagaki et al. [2], by mixing the kanemite powder with the 0.1 M aqueous solution of hexadecyltrimethylammonium bromide and adjusting pH to 11.5 by addition of NaOH. The mixture was heated to 70 °C and stirred for 3 h. Afterwards the pH was lowered to 8.5 by dropwise addition of 1 M HCl and the mixture stirred for further 3 h. The FSM-16 product was filtered, washed and dried in air. The template was removed by calcination at 550 °C for 6 h. Directly aluminated materials were obtained by addition of required amount of $Al(NO_3)_3{\cdot}9H_2O$ to the mixture of NaOH and SiO_2, at the stage of kanemite preparation, and continuing the synthesis as described above. Post-synthesis alumination consisted in impregnation of purely siliceous FSM-16 with a required amount of $Al(NO_3)_3{\cdot}9H_2O$ dissolved in a small quantity of water, followed by drying at 80 °C and calcination for 1.5 h at 550 °C. The directly and the post-synthesis aluminated samples are referred to as Al-FSM-16(x)/D and Al-FSM-16(x)/P, respectively, where x is the Si/Al ratio (x = 20, 40 or 60). The purely siliceous FSM-16 sample is denoted FSM-16. Transformation of the as received Al-FSM-16(x)/D into hydrogen form was carried out by subjecting the solids to exchange with ammonium cations (from NH_4NO_3 solution), followed by washing, drying and thermal decomposition of NH_4^+ species at 400 °C for 6 h. The hydrogen-forms are denoted H-Al-FSM-16(x)/D.

2.2. Methods

X-ray diffraction (XRD) patterns were recorded with a Philips 1710 powder diffractometer using Ni-filtered Cu Kα radiation. Transmission electron microscopic (TEM) studies were performed with FEI Tecnai G^2 transmission electron microscope at 200 kV. Chemical analysis was carried out with an Orbis Micro-EDXRF analyzer with a Rh anode as X-ray source (operating at 30 kV and 500 mA) and Si(Li) detector, using Orbis Vision software. BET specific surface area and pore size distribution based on non-local density functional theory were determined from the nitrogen adsorption-desorption isotherms obtained at −196 °C with a Quantachrome Nova 2000 apparatus. Prior to the measurement the samples were outgassed for 18 h at 200 °C. Solid state MAS-NMR spectra were measured on a home-made pulse NMR spectrometer at the magnetic field of 7.05 T. A Bruker HP-WB high-speed MAS probe equipped with the 4 mm zirconia rotor and KEL-F cap was used to record the MAS spectra at 8 kHz spinning

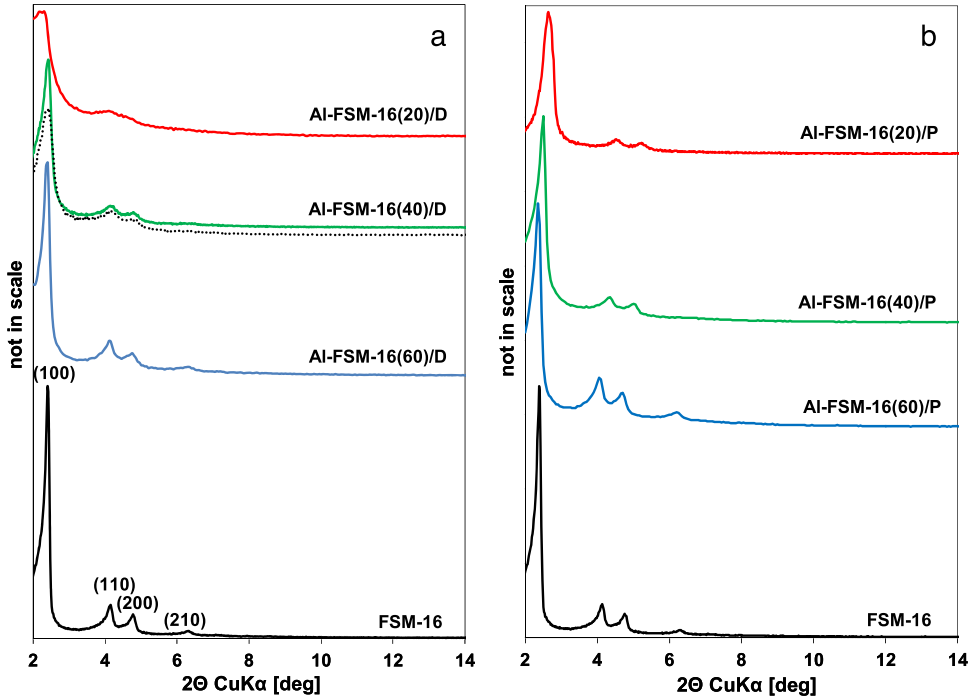

Fig. 1. XRD patterns of aluminated FSM-16 solids: a) direct method (dotted line: H-Al-FSM-16(40)/D sample), b) post-synthesis treatment.

speed. The ^{27}Al MAS-NMR spectra were measured at 78 MHz, using a single 2 μs radio-frequency pulse, corresponding to π/6 flipping angle. The acquisition delay used in accumulation was 1 s, and the number of acquisitions was equal to 2000. The frequency scale in ppm was referenced to the ^{27}Al resonance of 1 M aqueous solution of $Al(NO_3)_3$. The ^{29}Si MAS NMR spectra were measured at 59.517 MHz, using a single 3 μs radio-frequency pulse, corresponding to π/2 flipping angle. The acquisition delay used in accumulation was 60 s, and 256 scans were acquired. The frequency scale in ppm was referenced to the ^{29}Si resonance of tetramethylsilane (TMS). X-ray Photoelectron Spectroscopy (XPS) spectra were obtained with a hemispherical analyzer (SES R4000, Gammadata Scienta, pass energy 100 eV) and Mg Kα X-ray source (1254 eV), for powders pressed into indium foil. The electron binding energy scale (BE) was calibrated for maximum of C 1 s core excitation at 285.0 eV. Temperature programmed desorption of ammonia (NH_3-TPD) was studied in a flow microreactor system equipped with a QMS detector (Stanford Research, RGA 200), by monitoring the $m/z = 16$ line and $m/z = 17$ line, corrected for the contribution from water mass spectrum. Prior to NH_3 sorption the sample was outgassed in a flow of pure argon at 400 °C for 1 h. Subsequently, the microreactor was cooled down to 80 °C and the sample was saturated in a flow of NH_3 for about 30 min. Then, the sample was purged with argon flow at 100 °C until a constant baseline level was attained. Desorption was carried out with a linear heating rate (10 °C/min) in a flow of pure argon, in the temperature range 100–650 °C, at a 10 °C/min heating rate. FTIR study of pyridine adsorption (POCh Gliwice, analytical grade, dried over 3A molecular sieve) was carried out using self-supporting pellets of mesoporous silica samples placed in a quartz cell equipped with CaF_2 windows, designed to perform measurements at different temperatures. Prior to pyridine adsorption, the sample was outgassed at 400 °C under vacuum for 1 h. Then the cell was cooled to room temperature and the spectrum of activated sample was obtained. Later the sample was allowed to interact with pyridine at room temperature. Thereafter the cell with a sample was outgassed for 30 min under vacuum at 150 °C, 250 °C, and 350 °C. After cooling down, FTIR spectra of the samples were measured. For each measurement 64 scans were taken with a resolution of 2 cm^{-1} using a Nicolet 710 FTIR spectrometer. Concentrations of Brønsted acid sites, Lewis acid sites, and hydrogen-bonded pyridine were calculated (in μmol/g) on the basis of the intensities of the 1547 cm^{-1}, 1455 cm^{-1} and 1445 cm^{-1} bands, respectively, as described by Emeis [48]. Catalytic decomposition of ethanol was carried out in a fixed bed flow microreactor in the temperature range 150–350 °C, at a heating rate 2 °C/min, using 0.3 ml (ca. 0.15 g) of the catalyst. Prior to the experiment the catalyst was activated for 1 h at 350 °C in the flow of pure helium. The concentration of ethanol in the helium carrier gas was 6%. The reaction products were analyzed with a Perkin Elmer GC equipped with a Porapak column and FID.

3. Results and discussion

3.1. Structural characterization

Fig. 1a and b shows the results of XRD analysis of as received calcined aluminated FSM-16 samples prepared by direct and post-synthesis method. Comparison of the diagrams reveals some structural differences between both types of materials. The XRD pattern of purely siliceous sample FSM-16 shows four well resolved peaks, which are assigned to the (100), (110), (200) and (210) reflections of the hexagonal FSM-16 lattice. Insertion of aluminium by means of direct synthesis results in a gradual broadening of XRD peaks, so that in the most heavily doped Al-FSM-16(20)/D material the reflections other than (100) are barely resolved (Fig. 1a). In the post-synthesis aluminated samples, whose structural skeleton is determined by the parent purely siliceous FSM-16 material, a certain peak broadening upon Al incorporation is also observed, but at all levels of doping the post-synthesis aluminated samples show better structural order than the directly aluminated ones of comparable Al content (Fig. 1b). This observation is similar to the findings reported for the alumination of MCM-41 mesoporous silicas, which indicated that post-synthesis alumination provided materials with a better structural integrity than the direct method [24–28]. The loss of XRD resolution upon post-synthesis alumination may be due, in part, to the abrasive action of acidic aluminium nitrate solution.

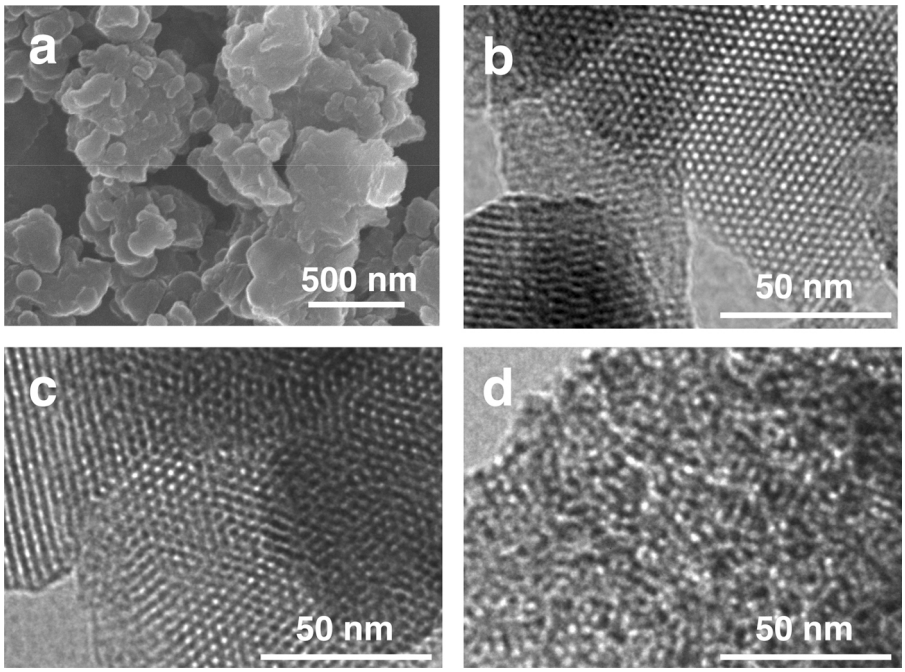

Fig. 2. a) SEM image of FSM-16, b) TEM image of FSM-16, c) TEM image of Al-FSM-16(20)/P, d) TEM image of Al-FSM-16(20)/D.

The reason for the loss of resolution observed in the directly aluminated samples is revealed in TEM experiment (Fig. 2b–d). TEM images of purely siliceous FSM-16 show the characteristic parallel arrangement of uniform channels which, when viewed along the channel axis form a hexagonal honeycomb structure (Fig. 2b). TEM micrograph of the post-synthesis aluminated Al-FSM-16(20)/P sample (Fig. 2 c) shows that the hexagonal ordering of mesopores is quite well maintained, although it appears more faulty than in the parent FSM-16. On the other hand, the TEM image of directly aluminated Al-FSM-16(20)/D sample shows that, while the channels retain a pretty uniform width, the hexagonal ordering appears only locally, with no long range arrays being formed (Fig. 2d). The effect indicates that the use of Al-containing kanemite hampers the self-assembly process and produces, in consequence, less ordered materials.

3.2. Textural characterization

Different impact of direct vs. post-synthesis alumination on the structure of FSM-16 solids is also reflected in the way alumination affects the nitrogen sorption/desorption isotherms (Fig. 3). All isotherms are of type IV, as expected for ordered mesoporous solids, with hysteresis loops of H3 type, typically generated by adsorption on aggregates of platy particles [49]. Indeed, SEM micrographs evidence the fine plate-like grain morphology of the samples, as illustrated in Fig. 2 a. In the case of directly aluminated materials, the growing content of Al brings about a gradually increasing downward shift of the isotherms, the effect accompanied by a decrease of the specific surface area (Fig. 3a, Table 1). Pore size distribution curves indicate the presence of uniform pores with maximum pore values (3.7 nm) slightly bigger than in the purely siliceous sample (3.5 nm) (Table 1). In the FSM-16 material the average pore size is 3.9 nm, which is close to the dominant pore radius and shows that the overall porosity is determined by the presence of template-generated channels. The data in Table 1 show that with the increasing Al content the difference between the maximum pore diameter and the average pore size increases, indicating that the loss of structural order generates some porosity other than that built around the rod-like micellar templates. In the post-synthesis aluminated samples, a downward shift of isotherms with respect to that of the purely siliceous material is also observed (Fig. 3 b). Analysis of pore size distribution shows that impregnation with Al results in a slight shift of PSD profiles towards lower pore sizes, and in the appearance of a shoulder (Al-FSM-16(60)/P) or a second maximum (Al-FSM-16(40)/P, Al-FSM-16(20)/P) at 3.2 nm, i.e. lower than the 3.5 nm found in the parent FSM-16 (Fig. 3d). The result is consistent with the partial pore filling upon impregnation with Al. In addition, in the case of Al-FSM-16(20)/P sample, the PSD curve indicates a certain build up of porosity above 4 nm, reflected also in an increase of the average pore diameter

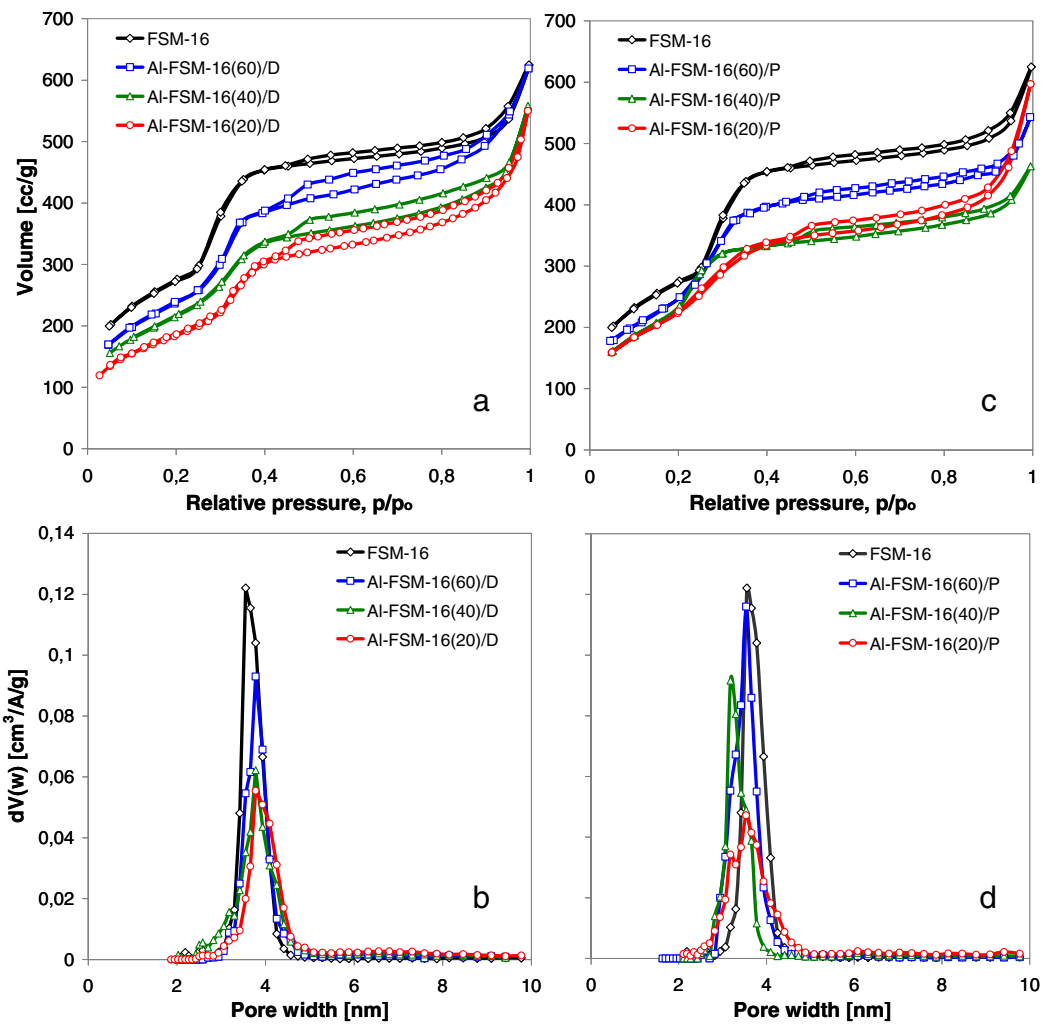

Fig. 3. Nitrogen adsorption/desorption isotherms and pore size distribution curves for directly aluminated (a and b, respectively) and post-synthesis aluminated (c and d, respectively) FSM-16 materials.

Table 1
Physicochemical characteristics of FSM-16 solids: d_{100} spacing, hexagonal lattice parameter a_0, S_{BET}—BET specific surface area, D_{max}—NL-DFT pore size maximum, D_{av}—average pore diameter, V_{tot}—total pore volume at $P/P_0 = 0.995$, Si/Al ratio from XRF and XPS.

Sample	d_{100} (nm)	a_0 (nm)	S_{BET} (m^2/g)	D_{max} (nm)	D_{av} (nm)	V_{tot} (cm^3/g)	Si/Al XRF	Si/Al XPS
FSM-16	3.7	4.3	1002	3.5	3.9	0.969	–	–
Al-FSM-16(60)/D	3.7	4.3	872	3.7	4.3	0.958	67	88
Al-FSM-16(40)/D	3.7	4.3	794	3.7	4.4	0.865	44	52
Al-FSM-16(20)/D	4.0	4.6	684	3.7	5.0	0.856	23	40
Al-FSM-16(60)/P	3.8	4.4	864	3.5	3.9	0.842	62	25
Al-FSM-16(40)/P	3.7	4.3	841	3.2	3.4	0.717	43	20
Al-FSM-16(20)/P	3.4	3.9	817	3.5	4.5	0.924	22	12

(Table 1). This effect, combined with the observed increase of the overall pore volume, is most likely due do to the corrosive action of the acidic environment during impregnation with Al.

3.3. Distribution and localization of aluminium

3.3.1. XPS and XRF spectroscopies

XRF and XPS analyses of the synthesized solids aimed at comparison of bulk *vs.* surface Si/Al ratio of aluminated materials. The appropriate data are gathered in Table 1. It is evident that the mode of Al distribution in the FSM-16 silica framework differs, depending on the adopted method of alumination. Thus, for the directly aluminated materials, the surface Si/Al ratio is higher than the bulk value, which points to a relative depletion of the surface region of the Al dopant. In contrast, the surface of post-synthesis aluminated samples is significantly enriched in aluminium with respect to the average composition. The latter obviously results from the nature of the impregnation procedure in which the Al source is first in contact with the outer surface of the purely siliceous FSM-16, and only then may penetrate the pore system. On the other hand, relative depletion of aluminium found for directly aluminated materials may be rationalized by recalling the mechanism of FSM-16 formation [40–42]. Transformation of kanemite, exchanged with hexadecyltrimethylammonium cations, to FSM-16, occurs through ordering of fragmented anionic silicate sheets into an intermediate layered silica-surfactant mesophase, which then, upon lowering of pH, evolves into the hexagonal structure. In the case of the Al-containing kanemite exchanged with hexadecyltrimethylammonium cations, the interlayer surfactant cations interact stronger with its Al-bearing fragments, showing a deficit of the positive charge. In consequence, during the stage of rod-like micelles formation, the Al-containing silicate species tend to accumulate at the organic/inorganic interface, resulting in the preferential Al siting at the inner pore walls of the final Al- FSM-16 structure.

3.3.2. Solid state ^{27}Al and ^{29}Si MAS-NMR spectroscopy

^{27}Al MAS NMR reveal further differences between the directly and the post-synthesis aluminated samples. This is illustrated in Fig. 4 a which shows, as an example, the spectra recorded for solids with Si/Al = 20. In both types of materials an absorption with the maximum in the range of $\delta = 52$ ppm is observed, characteristic of tetrahedrally coordinated Al sites, which confirms substitution of Al for Si in the mesoporous silica network [50]. In the post-synthesis aluminated sample, next to the dominant $\delta = 52$ ppm resonance line, a signal of lower intensity at ca. $\delta = 0$ ppm is visible, indicating that upon Al impregnation some of the inserted Al forms non-framework, octahedrally coordinated species. The lack of any such signal in the directly aluminated samples shows that this method of preparation leaves no detectable extra-lattice Al.

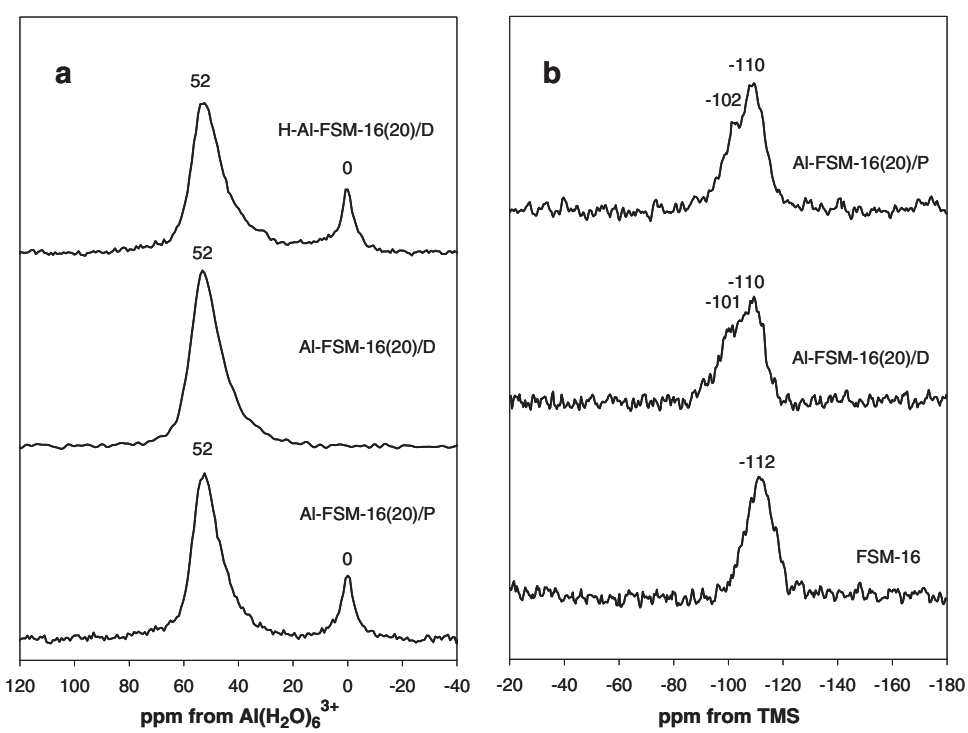

Fig. 4. a) ^{27}Al MAS NMR and b) ^{29}Si MAS NMR spectra of aluminated FSM-16 materials.

However, the procedure of converting the directly aluminated materials into their hydrogen forms is associated with a certain degree of dealumination, as evidenced by ^{27}Al MAS NMR spectrum of the H-Al-FSM-16(20)/D sample (Fig. 4a). A similar effect has been reported for directly aluminated MCM-41 silica [26]. Analysis of ^{29}Si MAS NMR resonance of aluminated samples confirms that incorporated aluminium is indeed substituting the Si centres in the mesoporous silica [50]. The spectrum of purely siliceous sample shows a single line with chemical shift of $\delta = -112$ ppm, characteristic of Q^4(0Al) units, in which the central Si atom is interconnected via four oxygen bridges with other Si atoms. A certain asymmetry of this absorption indicates a small contribution from less condensed Si species. Insertion of Al is associated with the appearance of a second maximum at less negative δ values (Fig. 4b). Its position, at $\delta = -101$ and -102 ppm, in Al-FSM-16(20)/D and Al-FSM-16(20)/P, respectively, points to the contribution from tetrahedrally coordinated Si Q^4(1Al) units, in which one of four bridging oxygen connects the Si center with an Al site. It should be noted that the ^{29}Si MAS-NMR spectra have much poorer signal to noise ratio than the ^{27}Al ones. This is caused by the difference in natural abundances of both isotopes, which are respectively 4% and 100%, and equally large difference in T_1 relaxation times. Nevertheless, the quality of ^{29}Si MAS-NMR spectra is sufficient for unequivocal interpretation.

3.3.3. Infrared spectroscopy

Fig. 6 shows the framework vibration region of FTIR spectra recorded for FSM-16, Al-FSM-16(20)/D, Al-FSM-16(20)/P, and H-Al-FSM-16(20)/D. The most prominent band in the vicinity of 1080 cm^{-1}, the band at 1243 cm^{-1} and a weak peak around 1198 cm^{-1} are due to asymmetric Si—O stretching modes within SiO_4 tetrahedra. The less intense feature at 798 cm^{-1} is due to symmetric stretching Si—O modes, and the band at 456 cm^{-1} is associated with bending skeletal modes [51]. Around 960 cm^{-1}, a band assigned to Si-O stretching within terminal Si—OH groups, is observed [52]. In addition, in the spectrum of FSM-16 and post-synthesis aluminated Al-FSM-16(20)/P, a weak band is visible at 620 cm^{-1}. This band is absent in the directly aluminated materials (Fig. 5). Analysis of other characteristic frequencies confirms that alumination affects the silica network in a different way, depending on the manner of Al insertion. Direct alumination shows a clear impact on the framework vibrations. All stretching bands become broader, and, as a result, the 1243 cm^{-1} and 1198 cm^{-1} peaks resolved in FSM-16, coalesce into a shoulder in Al-FSM-16(20)/D. A downward shift of the dominant maximum from 1087 cm^{-1} to 1077 cm^{-1} is observed, indicative of the Al for Si substitution and formation of the aluminosilicate framework. Noteworthy, the band at 960 cm^{-1} due to Si—O stretches within terminal silanols becomes less pronounced, although this bonding is not directly affected by Al substitution. Transformation of Al-FSM-16(20)/D into its hydrogen form does not change the spectrum of framework vibrations in any meaningful way. In contrast to direct alumination, the post-synthesis incorporation of Al has practically no effect on the FTIR detectable skeletal vibrations of parent FSM-16. The only exception is the suppression of the 960 cm^{-1} band associated with free silanols. In order to get more insight into this effect, FTIR spectra in the O—H stretching mode range were analyzed (Fig. 6)

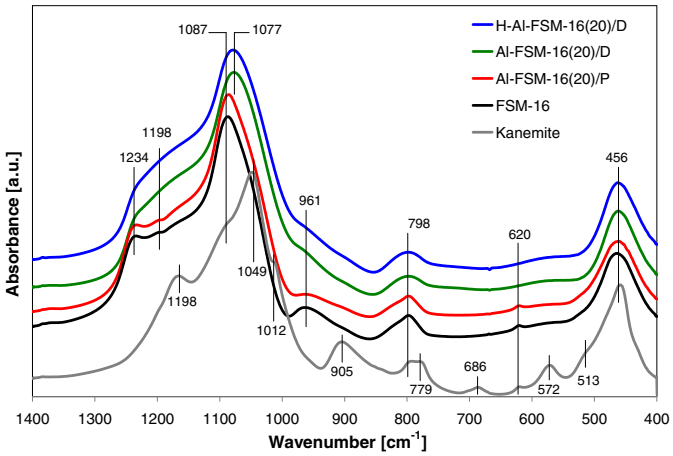

Fig. 5. FTIR spectra of the skeletal vibrations in aluminated FSM-16 materials.

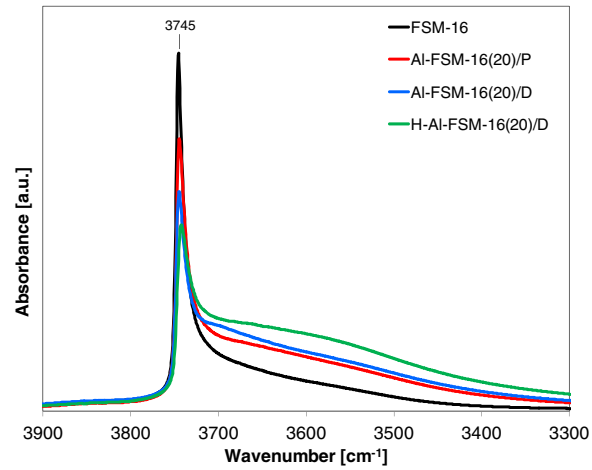

Fig. 6. FTIR spectra of the O—H stretching mode region in aluminated FSM-16 materials.

The sharp band at 3745 cm^{-1} is due to free silanol groups [53], while the broad band in the 3700–3300 cm^{-1} range to hydrogen bonded hydroxyls, associated mainly with defects caused by interrupted Si—O—Si linkages [54]. It is evident that both the direct and the post-synthesis alumination result in a decrease of the 3745 cm^{-1} band intensity, which explains the diminution of the 960 cm^{-1} band in the skeletal modes range. In addition, both types of alumination cause an increase of the broad band intensity, which signifies enhanced contribution from H-bonded OH-groups, and reflects an increased concentration of surface structural defects in the aluminated silica framework. Transformation of Al-FSM-16(20)/D into its hydrogen form brings about further increase of the broad band intensity. Obviously, the partial loss of Al from the mesoporous silica structure, occurring in the process of H-Al-FSM-16(20)/D preparation and evidenced by ^{27}Al MAS NMR, leads to a higher content of structural defects, including the hydroxylated ones.

3.4. Acidic properties

As indicated in the introduction, formation of Si–O–Al linkages in the silica-based solids is a means of enhancing the materials acidity. In order to follow changes in the acidic properties of FSM-16 induced by its alumination, adsorption/desorption of base probe molecules, i.e. ammonia and pyridine, has been carried out. The acidity study was completed with tests of the solids activity in the catalytic decomposition of ethanol.

3.4.1. Ammonia TPD-MS study

Substitution of Al for Si in the silica framework generates cation exchange positions, which, when occupied by protons, are the source of Brønsted acidity. Surface coordinatively unsaturated Al sites may act as Lewis acid sites. To get insight into the acidic

properties of aluminated FSM-16 samples the temperature programmed desorption of ammonia, which probes jointly the Brønsted and the Lewis acidity, has been carried out. The TPD curves presented in Fig. 7 show that the investigated samples possess very different characteristics. Thus, purely siliceous FSM-16 has no meaningful concentration of sites capable of interaction with ammonia. The as-received directly aluminated samples are not expected to hold large amount of ammonia, due to the neutralizing effect of sodium incorporated during synthesis carried out at strongly basic environment maintained by addition of NaOH. Indeed, the Al-FSM-16(x)/D series shows low intensity NH_3 TPD profiles, with more ammonia desorbing from samples with larger Al content. Two broad, flat maxima, centered around 360 and 560 °C may be discerned, showing that the acidity remaining in the Na-containing samples is of medium and strong character [55]. Much more ammonia is desorbed from the H-Al-FSM-16(20)/D sample, obtained from Al-FSM-16(20)/D whose acidity has been regenerated by exchange with NH_4^+ ions followed by calcination. The broad thermodesorption peak with flat maximum centered around 340 °C points to a build-up of a spectrum of medium strong acid sites. In the case of post-synthesis alumination, the impregnatiom of the parent, purely siliceous sample is carried out in the acidic environment, so that the acidity generated by Al substitution is not obscured by neutralizing effect of basic cations. As a result, the TPD profiles of Al-FSM-16(x)/P series are significantly higher than those of the as-received directly aluminated counterparts, with capacity for ammonia sorption growing with the Al content. The curves are dominated by the maximum at 360 °C and tail off in the direction of high temperature desorption, indicating a contribution from strong acid centers capable of holding ammonia up to 500–600 °C. Noteworthy, the total acidity of H-Al-FSM-16(20)/D is significantly lower than that of the Al-FSM-16(20)/P sample, and part of its acid centers represents weaker acidity, as indicated by a shift of its TPD profile to lower temperature. Both effects show that the post-synthesis alumination represents a more efficient means of introducing the acid function into the FSM-16 mesoporous silica than the direct method, similarly as has been previously observed in the case of MCM-41 mesoporous silicas [20,21,27].

3.4.2. FTIR study of pyridine adsorption/desorption

Adsorption/desorption of pyridine monitored by FTIR spectroscopy was used to identify the nature of acid sites present in FSM-16 and its aluminated derivatives. Key information required for the identification of various pyridine species can be found in the 1650–1400 cm^{-1} range of IR spectrum, where absorption bands assigned to ring vibrations (C—C and C—N skeletal modes) of pyridine appear [56]. For pyridinium ion, which results from the transfer of an acidic proton from the surface Brønsted site to the pyridine molecule, a diagnostic band near 1540 cm^{-1} due to N^+—H vibration is observed, accompanied by ring vibrations at 1485–1500 cm^{-1}, around 1620 cm^{-1}, and 1640 cm^{-1}. For pyridine bound to Lewis acid sites the most prominent IR bands are located at 1447–1460 cm^{-1}, 1488–1503 cm^{-1}, and in the 1600–1633 cm^{-1} range. Hydrogen bonding of pyridine to weakly acidic surface hydroxyls gives rise to bands at 1440–1447 cm^{-1}, 1485–1490 cm^{-1}, and 1580–1600 cm^{-1}.

Results of interaction with pyridine are reported for four samples: purely siliceous FSM-16, Al-FSM-16(20)/P, Al-FSM-16(20)/D, and the hydrogen form of the latter, H-Al-FSM-16(20)/D. Fig. 8 shows the 1650–1400 cm^{-1} region of FTIR spectra recorded after exposure to pyridine vapour and subsequent evacuation at 150, 250, and 350 °C. At the lowest temperature of outgassing, the purely siliceous material shows bands at 1445 and 1599 cm^{-1}, which indicate the presence of pyridine hydrogen-bonded to weakly acidic silanols (Fig. 8a). Low intensity bands around 1455 and 1490 cm^{-1} point to the presence of a trace amount of Lewis acid sites. The H-bonded pyridine is quite unstable and the intensities of the relevant bands decrease strongly upon outgassing at 250 °C, and practically disappear after evacuation at 350 °C. FTIR spectra of pyridine adsorbed at Al-FSM-16(20)/P sample, shown in Fig. 8b, evidence a major change in the surface properties of

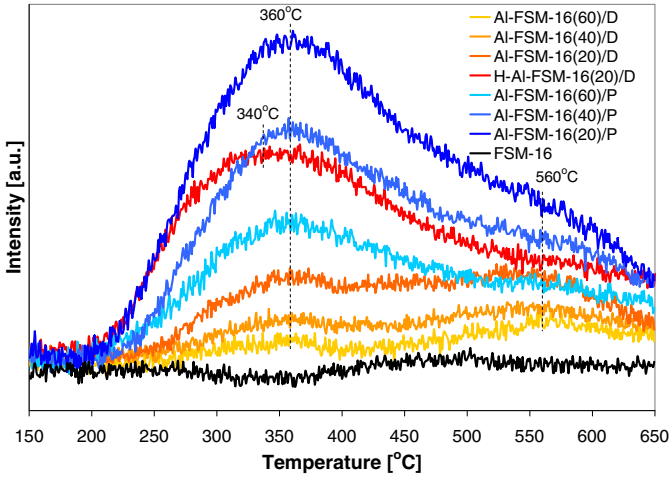

Fig. 7. NH_3-TPD profiles of aluminated FSM-16 materials.

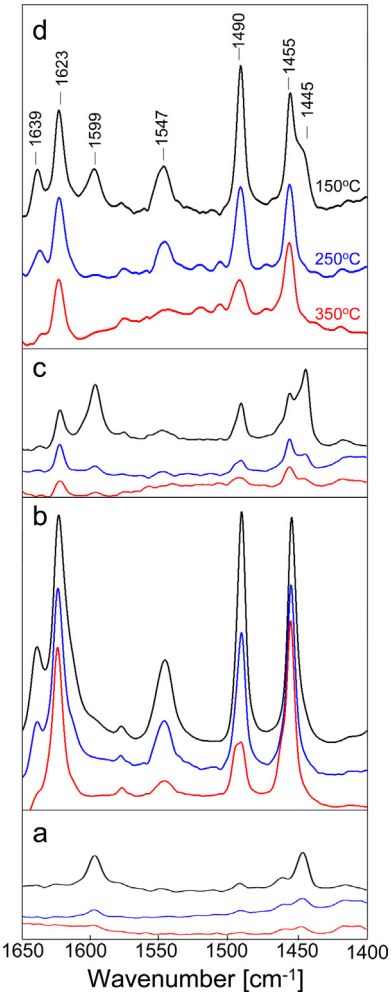

Fig. 8. FTIR spectra of pyridine adsorbed on aluminated FSM-16 materials: a) FSM-16, b) Al-FSM-16(20)/P, c) Al-FSM-16(20)/D, d) H-Al-FSM-16(20)/D.

Table 2
Concentrations of Brønsted acid sites, Lewis acid sites, weakly acidic silanols, and B/L—Brønsted to Lewis acid sites ratio from FTIR study of pyridine adsorption/desorption. In brackets% of acid centers with respect to number of sites detected at 150 °C.

Sample	Outgassing temperature [°C]	Brønsted acid sites [μmol g^{-1}]	Lewis acid sites [μmol g^{-1}]	Weakly acidic silanols [μmol g^{-1}]	B/L
FSM-16	150	–	4	32	–
	250	–	3	9	–
	350	–	2	6	–
Al-FSM-16(20)/D	150	16	36	56	0.44
	250	8	20 *(56%)*	12	0.40
	350	–	16 *(44%)*	8	–
H-Al-FSM-16(20)/D	150	78	99	52	0.79
	250	42 *(54%)*	84 *(85%)*		0.50
	350	16 *(21%)*	83 *(84%)*	–	0.19
Al-FSM-16(20)/P	150	192	236	–	0.81
	250	104 *(54%)*	200 *(85%)*	–	0.52
	350	36 *(19%)*	196 *(83%)*	–	0.18

FSM-16 solid subjected to post-synthesis alumination. Very strong bands at 1455 and 1623 cm^{-1} are indicative of pyridine bonded coordinatively to Lewis acid centers, the 1547 and 1639 cm^{-1} bands are associated with the pyridinium cations formed by interaction with Brønsted acid sites, and the intense 1491 cm^{-1} band is generated by both types of chemisorbed pyridine. Evacuation at higher temperatures shows that Brønsted acid sites are less thermally stable than the Lewis ones, indicating high strength of the latter. In consequence, the ratio of Brønsted to Lewis acidity decreases with increasing temperature (Table 2). A characteristic feature of the spectra is the lack of H-bonded pyridine, which suggests that weakly acidic silanols present at the surface of purely siliceous FSM-16 participate in Al anchoring carried out by means of post-synthesis alumination and/or are screened by the deposited Al species. FTIR analysis of pyridine adsorbed on the directly aluminated Al-FSM-16(20)/D solid and evacuated at 150 °C shows, in agreement with the NH_3 TPD data, that the material has a significantly lower acidity than the post-synthesis aluminated sample (Fig. 8c). The spectrum is dominated by the 1445 and 1599 cm^{-1} bands characteristic of H-bonded pyridine. The maximum at 1547 cm^{-1}, indicative of Brønsted acid sites, is barely visible, as expected for Na-neutralized material, and the 1455 cm^{-1} band associated with the Lewis acidity is much less intense than in the Al-FSM-16(20)/P sample. Upon evacuation at higher temperatures H-bonded pyridine and traces of pyridinium ions disappear more rapidly than pyridine bound to Lewis centers, so that weak 1455 cm^{-1} and 1623 cm^{-1} bands associated with the latter are the main features of the low intensity spectrum of sample outgassed at 350 °C. The spectrum of the H-Al-FSM-16(20)/D sample after evacuation of pyridine at 150 °C shows that transformation of the as-received directly aluminated material to its hydrogen form generates acidity of both types, as evidenced by the presence of distinct 1455 cm^{-1} and 1547 cm^{-1} bands of pyridine adsorbed at Lewis and Brønsted acid sites, respectively (Fig. 8d). In addition, the shoulder at 1447 cm^{-1} indicates the presence of H-bonded pyridine species. The data in Table 2 show that the Brønsted to Lewis acid sites ratio in H-Al-FSM-16(20)/D increases with respect to the Al-FSM-16(20)/D sample, the effect consistent with the replacement of sodium cations by protons. As in other samples, the pyridine-Lewis acid site ensembles are more resistant to outgassing at higher temperatures than the pyridinium cations or H-bonded pyridine (Table 2). Comparison of thermal stabilities of pyridine species bound to Brønsted and Lewis acid sites, estimated from the fraction of relevant species retained upon evacuation at increasing temperatures (Table 2), shows that while in both types of aluminated materials Lewis acidity is stronger than the Brønsted one, there is no meaningful difference between the hydrogen form of directly aluminated FSM-16 and the post-synthesis aluminated sample as far as the strength of a particular type of acid sites is concerned. As a result, the evolution of the Brønsted to Lewis acidity ratio with temperature of thermal treatment is similar for H-Al-FSM-16(20)/D and Al-FSM-16(20)/P.

3.4.3. Catalytic decomposition of ethanol

The materials acidity has also been evaluated by investigation of ethanol decomposition, a catalytic test reaction sensitive to the acid-base properties. Ethanol may decompose to yield dehydration (ethylene, diethyl ether) and/or dehydrogenation (acetaldehyde) products, the former being formed preferentially on acid sites, the latter favored on basic/redox centers [57]. The investigated series included FSM-16, Al-FSM-16(20)/D, H-Al-FSM-16(20)/D and Al-FSM-16(20)/P. The activity in ethanol decomposition and the product distribution varied with the catalyst composition. In Fig. 9 the conversion and the selectivities to different products observed at 300 °C are compared for all tested catalysts. The FSM-16 and the as received Al-FSM-16(20)/D samples show poor activity and the main reaction product is acetaldehyde. In contrast, the hydrogen form of the directly aluminated material, H-Al-FSM-16(20)/D, and the post-synthesis aluminated sample Al-FSM-16(20)/P are much more active and yield dehydration products, mainly ethylene and some diethyl ether. The results of catalytic tests are consistent with the outcome of acidity studies by means of probe molecules adsorption/desorption. On the essentially non-acidic and/or poorly acidic samples such as FSM-16 and Al-FSM-16(20)/D, the activity is low and only the dehydrogenation pathway is observed, catalyzed

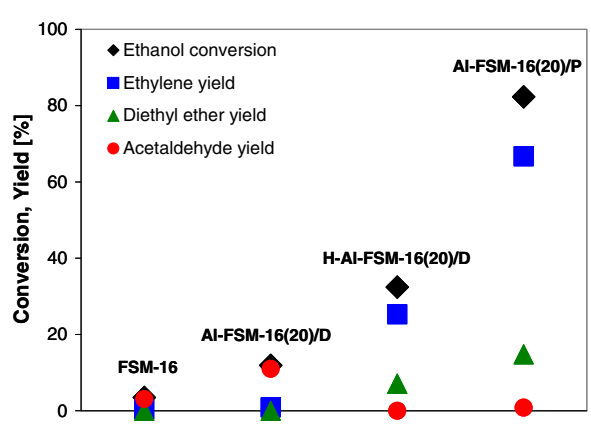

Fig. 9. Ethanol conversion and yield to decomposition products at 300 °C over aluminated FSM-16 solids.

presumably by the basic sites associated with the residual sodium. On the other hand, on H-Al-FSM-16(20)/D and Al-FSM-16(20)/P samples, possessing both the Brønsted and the Lewis acid sites, the dehydration pathway becomes viable, and the activity increases, the more the higher the catalyst acidity.

4. Conclusions

Our work revealed significant differences in physico-chemical characteristics of directly and post-synthesis aluminated FSM-16 materials. It is apparent that direct alumination method is more efficient in insertion of Al into substitutional positions of silica, than the post-synthesis one, which, as demonstrated by ^{27}AlMAS NMR, leaves part of the introduced Al in extra-framework positions. However, this advantage is lost upon transformation of the as-received directly aluminated materials into their hydrogen forms, since the procedure is invariably associated with expulsion of some Al from sites within mesoporous silica lattice. Direct Al insertion introduces a higher degree of structural disorder both in the long-range hexagonal packing, as revealed by XRD and TEM, and the short and medium range atomic array, as evidenced by FTIR. Further structural defects involving broken Si-O-Si linkages are generated upon transformation of directly aluminated samples into their hydrogen forms. Differently aluminated materials differ also in the spatial distribution of introduced Al. Combined XPS and XRF analyses show that the surface regions of directly aluminated materials are relatively depleted of Al, while the surface of post-synthesis aluminated samples is significantly enriched in aluminium. This finding has implications for design of FSM-16 based sorbents and/or catalytic materials, since in directly aluminated materials the sites capable of cation exchange are preferentially located at, or near to, inner pore walls, while in the in post-synthesis aluminated solids they are present mainly at the external surface. As expected, alumination generates acidic properties, which in the case of directly aluminated samples are fully revealed only after transformation into the hydrogen forms. All tests of acidity show that post-synthesis alumination is a more efficient means of introducing acid sites into the FSM-16 lattice. The generated acidity is of Brønsted and Lewis nature. Lewis acid sites are stronger than Brønsted ones, but the strength of a particular type of acid sites is comparable in both types of materials.

Acknowledgements

This work received funding from the Marian Smoluchowski Krakow Research Consortium—a Leading National Research Centre KNOW supported by the Polish Ministry of Science and Higher Education, AGH University of Science and Technology project 11.11.140.319, and from the Polish Ministry of Science and Education project 2 P04D 050 26.

References

[1] J.S. Beck, J.C. Vartuli, W.J. Roth, M.E. Leonowicz, C.T. Kresge, K.D. Schmitt, C.T.W. Chu, D.H. Olson, E.W. Sheppard, J. Am. Chem. Soc. 114 (1992) 10834–10843.
[2] S. Inagaki, Y. Fukushima, A. Okada, T. Kurauchi, K. Kuroda, C. Kato, in: R. von Ballmoos, J.B. Higgins, M.M.J. Treacy (Eds.), Proc. 9th Int. Zeolite Conf., Vol. I, Butterworth-Heineman, Montreal, 1992, pp. 305–311.
[3] S. Inagaki, Y. Fukushima, K. Kuroda, Chem. Commun. (1993) 680–682.
[4] C.-Y. Chen, H.X. Li, M.E. Davis, Microporous Mater. 2 (1993) 17–26.
[5] A. Corma, V. Fornés, M.T. Navarro, J. Pérez-Pariente, J. Catal. 148 (1994) 569–574.
[6] J.M. Kim, J.H. Kwak, S. Jun, R. Ryoo, J. Phys. Chem. 99 (1995) 16742–16747.
[7] R. Mokaya, W. Jones, Z. Luan, M.D. Alba, J. Klinowski, Catal. Lett. 37 (1996) 113–120.
[8] R.B. Borade, A. Clearfield, Catal. Lett. 31 (1995) 267–272.
[9] R. Mokaya, W. Jones, Chem. Commun. (1997) 2185–2186.
[10] H. Kosslik, H. Landmesser, R. Fricke, J. Chem. Soc. Faraday Trans. 93 (1997) 1849–1854.
[11] M.T. Janicke, C.C. Landry, S.C. Christiansen, S. Birtalan, G.D. Stucky, B.F. Chmelka, Chem. Mater. 11 (1999) 1342–1351.
[12] R. Mokaya, W. Jones, J. Mater. Chem. 9 (1999) 555–561.
[13] H. Kosslik, G. Lischke, B. Parlitz, W. Storek, R. Fricke, Appl. Catal. A: Gen. 184 (1999) 49–60.
[14] A. Matsumoto, H. Chen, K. Tsutsumi, M. Grün, K. Unger, Microporous Mesoporous Mater. 32 (1999) 55–62.
[15] S.-C. Shen, S. Kawi, J. Phys. Chem. B 103 (1999) 8870–8876.
[16] R. Mokaya, J. Phys. Chem. B 104 (2000) 8279–8286.
[17] M.M.L. Ribeiro Carrott, F.L. Conceição, J.M. Lopes, P.J.M. Carrott, C. Bernardes, J. Rocha, F. Ramôa Ribeiro, Microporous Mesoporous Mater. 92 (2006) 270–285.
[18] S. Li, Q. Xu, J. Chen, Y. Guo, Ind. Eng. Chem. Res. 47 (2008) 8211–8217.
[19] J.T. Tompkins, R. Mokaya, ACS Appl. Mater. Interfaces 6 (2014) 1902–1908.
[20] R. Ryoo, C.H. Ko, R.F. Howe, Chem. Mater. 9 (1997) 1607–1613.
[21] R. Mokaya, W. Jones, Chem. Commun. (1998) 1839–1840.
[22] S.C. Shen, S. Kawi, Langmuir 18 (2002) 4720–4728.
[23] S. Jun, R. Ryoo, J. Catal. 195 (2000) 237–243.
[24] L.Y. Chen, Z. Ping, G.K. Chuah, S. Jaenicke, G. Simon, Microporous Mesoporous Mater. 27 (1999) 231–242.
[25] Y. Liu, W. Zhang, T.J. Pinnavaia, J. Am. Chem. Soc. 122 (2000) 8791–8792.
[26] A. Ghanbari–Siahkali, A. Philippou, A. Garforth, C.S. Cundy, M.W. Anderson, J. Dwyer, J. Mater. Chem. 11 (2001) 569–577.
[27] S.K. Jana, H. Takahashi, M. Nakamura, M. Kaneko, R. Nishida, H. Shimizu, T. Kugita, S. Namba, Appl. Catal. A: Gen. 245 (2003) 33–41.
[28] T. Kugita, S.K. Jana, T. Owada, N. Hashimoto, M. Onaka, S. Namba, Appl. Catal. A: Gen. 245 (2003) 353–362.
[29] H. Du, V.V. Terskikh, C.I. Ratcliffe, J.A. Ripmeester, J. Am. Chem. Soc. 124 (2002) 4216–4217.
[30] R. Mokaya, ChemPhysChem 3 (2003) 360–363.
[31] R. Mokaya, Stud. Surf. Sci. Catal. 146 (2003) 435–438.
[32] M.A. Zanjanchi, Sh. Asgari, Solid State Ionics 171 (2004) 277–282.
[33] S. Inagaki, Y. Yamada, Y. Fukushima, Stud. Surf. Sci. Catal. 105 (1997) 109–115.
[34] H. Chen, A. Matsumoto, N. Nishimiya, T. Takeichi, K. Tsutsmi, Microporous Mesoporous Mater. 40 (2000) 289–298.
[35] Q. Kan, V. Fornés, F. Rey, A. Corma, J. Mater. Chem. 10 (2000) 993–1000.
[36] T. Selvam, V.R.R. Marthala, R. Herrmann, W. Schwieger, N. Pfänder, R. Schlögl, H. Ernst, D. Freude, Stud. Surf. Sci. Catal. 158 (2005) 501–508.
[37] T. Selvam, M. Köstner, G.T.P. Mabande, W. Schwieger, N. Pfänder, R. Schlögl, J. Porous Mater. 14 (2007) 263–272.
[38] M. Zimowska, A. Michalik–Zym, J. Połtowicz, M. Bazarnik, K. Bahranowski, E.M. Serwicka, Catal. Today 124 (2007) 55–60.
[39] D. Duraczynska, E.M. Serwicka, A. Drelinkiewicz, D. Rutkowska–Zbik, M. Witko, R. Socha, M. Zimowska, Z. Olejniczak, Appl. Catal. A: Gen. 427–428 (2012) 16–23.
[40] C.-Y. Chen, S.L. Burkett, H.-X. Li, M.E. Davis, Microporous Mesoporous Mater. 2 (1993) 27–34.
[41] J.C. Vartuli, C.T. Kresge, M.E. Leonowicz, A.S. Chu, S.B. McCullen, I.D. Johnson, E. W. Sheppard, Chem. Mater. 6 (1994) 2070–2077.
[42] T. Kimura, K. Kuroda, Adv. Funct. Mater. 19 (2009) 511–527 and the references therein.
[43] C.-Y. Chen, S.Q. Xiao, M.E. Davis, Microporous Mater. 4 (1995) 1–20.
[44] Y. Inaki, H. Yoshida, K. Kimura, S. Inagaki, Y. Fukushima, T. Hattori, PhysChemChemPhys 2 (2000) 5293–5297.
[45] N. Tada, Y. Matsusaki, T. Miura, A. Itoh, Chem. Pharm. Bull. 59 (2011) 906–908.
[46] A. Michalik–Zym, M. Zimowska, K. Bahranowski, E.M. Serwicka, Mineral. Polon. 38 (2007) 151–160.
[47] A. Michalik–Zym, M. Zimowska, E. Bielańska, K. Bahranowski, E.M. Serwicka, Mineral. Polon. 38 (2007) 161–170.
[48] C.A. Emeis, J. Catal. 141 (1993) 347–354.
[49] F. Rouquerol, J. Rouquerol, K. Sing, Adsorption by Powders and Porous Solids: Principles, Methodology and Applications, Academic Press, Lodon, San Diego, 1999 (Chapter 13).
[50] G. Engelhardt, D. Michel, High Resolution Solid State NMR of Silicates and Zeolites, Wiley, New York, 1987.
[51] E. Flanigen, H. Khatami, H.A. Szymanski, ACS Adv. Chem. Ser. 101 (1971) 201–229.
[52] M.A. Camblor, A. Corma, J. Pérez-Pariente, J. Chem. Soc. Chem. Commun. (1993) 557–559.
[53] T. Yamamoto, T. Tanaka, T. Funabiki, S. Yoshida, J. Phys. Chem. B 102 (1998) 5930–5939.
[54] H. Koslick, H. Landmesser, R. Fricke, J. Chem. Soc. Faraday Trans. 93 (1997) 1849–1854.
[55] H. Sato, Catal. Rev. Sci. Eng. 39 (1997) 395–424.
[56] E.P. Parry, J. Catal. 2 (1963) 371–379.
[57] A. Gervasini, A. Auroux, J. Catal. 131 (1991) 190–198.